# A solid state ultraviolet lasers based on cerium-doped $LiCaAlF_6$ crystal resonator

Nan Yu*[a], Thanh Le[a], Steven J. Schowalter[b], Wade Rellergert[b], Justin Jeet[b], Guoping Lin[a], Eric Hudson[b]

[a] Jet Propulsion Laboratory, California Institute of Technology, Pasadena, CA 91009, USA
[b]Department of Physics and Astronomy, University of California, Los Angeles, CA 90095, USA

## ABSTRACT

We report the first demonstration of a UV laser using a high-Q whispering gallery mode (WGM) resonator of Ce+: LiCaAlF6. We show that WGM resonators from LiCaAlF6 can achieve a Q of 2.6 x $10^7$ at UV. We demonstrated a UV laser at 290 nm with a pulsed pump laser at 266 nm. The experiments showed the low pump threshold intensity of 7.5 x $10^9$ W/$m^2$ and slope efficiency of 25%. We have also observed lasing delay dynamics. These results are consistent with our modeling and theoretical estimates, and pave the way for a low threshold cw UV laser using WGM resonator cavity.

**Keywords:** Whispering Gallery Mode Resonators, Ultraviolet Lasers

## 1. INTRODUCTION

Tunable single frequency and mode-locked laser sources in the ultraviolet (UV) region are widely used in a number of important applications, including molecular spectroscopy, detection of atmospheric constituents, and remote sensing [1-3]. Of particular high precision spectroscopy is the application in atomic frequency standards. Many current [4] and planned [5] optical clocks involve atomic transitions in the UV region. At present time, most UV laser systems operate either in pulsed mode or are obtained through nonlinear frequency conversion [6,7], as few viable UV gain media are known [8].

Solid state UV systems are of particular interests. Of the known UV gain media, trivalent cerium-doped colquiriites $Ce^{3+}$:$LiCaAlF_6$ possess several intriguing features, such as a convenient pumping wavelength (266 nm) and a gain bandwidth of 280-330 nm [9-11], allowing in principle both tunable cw and mode-locked operation. In additional, the cerium lasers inherit all advantages of solid-state crystalline lasers including high efficiency, indefinite material lifetime, tunable, simpler construction and compactness. To date however, neither cw nor broadband mode-locked lasing has been demonstrated in these systems [12], as the short lifetime of the upper state in the crystal requires pump power in excess of 1 W to reach the lasing threshold in traditional Fabry-Perot cavity designs [13].

We investigated an alternative approach that utilizes a dielectric resonator based on whispering gallery modes (WGM) in a circular dielectric medium. In a WGM resonator, light is trapped near the surface of the dielectric by repeated total internal reflection, and, when a low absorption material is used, a high quality (Q) factor can be realized. This high-Q resonator cavity, together with the small mode volume of a WGM resonator, leads to a significant reduction of the lasing pump power threshold [14-17] for continuous wave (cw) operation.

In this work, we report the first demonstration of a UV WGM laser. Using crystalline $LiCaAlF_6$ (LiCAF) as the host material, we have fabricated a WGM resonator with a Q in excess of $10^7$ at 370 nm. We have also experimentally investigated the properties of a Ce:LiCAF WGM laser with pulsed pumping and observed both low threshold lasing, as well as pulsed lasing time delay dynamics. Both the threshold measurements and delay dynamics were found in good agreement with our theoretical analyses. From these results, we calculate that it is possible to achieve a cw Ce:LiCAF WGM UV laser with a threshold pump power of 20 mW.

Updated 1 March 2012

## 2. THRESHOLD ESTIMATE AND DYNAMICS SIMULATION

Considerable efforts have been devoted to generate UV/VUV lasers based on $Ce^{3+}$ ions [8-11, 13]. Fluoride crystals are often used as cerium host material due to its wide band gap and high transparency in UV region [9]. Fig.1 shows the energy structure of $Ce^{3+}$:LiCAF crystal. $\sigma_{abs}$ is the absorption cross section for pump wavelength which shows the probability of an absorption process or the ability of the material to absorb the pump photon. $\sigma_{Em}$ determines the ability for an electron in upper laser level to transfer to lower lever and produces an additional photon. Electrons in upper laser level would absorb photons and be excited to conduction band of the host, which caused inefficiency for stimulated emission. This probability is $\sigma_{ESA}$. Thus the net gain related stimulated emission cross section is reduced, which is written as $\sigma_{eff} = \sigma_{Em} - \sigma_{ESA}$.

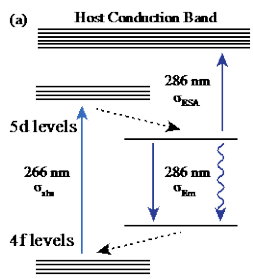


Figure 1: Schematic of the energy level structure in Ce:LiCAF crystal and related parameter designation.

We investigate a laser cavity system in which a WGM resonator is made entirely of Ce:LiCAF crystal material. To estimate the pumping threshold and also study the pump dynamics in this system, we write down the following rate equations for the 4-level laser scheme:

$$\frac{dN_2}{dt} = R_p - \frac{\sigma_{Em} I}{\hbar\omega_{Em}}(N_2 - N_1) - \frac{\sigma_{ESA} I}{\hbar\omega_{ESA}}(N_2 - N_{es}) - \Gamma_{21} N_2 \qquad (1)$$

$$\frac{d\phi}{dt} = -\frac{\phi}{\tau_c} + V_g \frac{\sigma_{Em} I}{\hbar\omega_{Em}}(N_2 - N_1) - V_g \frac{\sigma_{ESA} I}{\hbar\omega_{ESA}}(N_2 - N_{es}) - \Gamma_{21} N_2 V_g \qquad (2)$$

Field Code Changed

Field Code Changed

where $N_i$ is the number density of $Ce^{3+}$ ions in the $i^{th}$ level, $\Phi$ is the resonant photon number in the resonator, $R_p$ is the pumping rate constant, $V_g$ is the volume of the resonator that sees gain, $I$ is the resonant photon intensity in the cavity, $\tau_c$ is the cavity lifetime (loss rate) which is determined by the resonator quality factor $Q$ by the relationship

$$Q = \omega_s \tau_c = \frac{2\pi n c \tau_c}{\lambda_s} \qquad (3)$$

We can simplify this model by making a few assumptions. First, the rates $\Gamma_{32}$ and $\Gamma_{10}$ are large compared to $\Gamma_{30}$ and $\Gamma_{21}$ which allow us to approximate $N_2 >> N_3, N_1$. We can also assume that $N_2 >> N_{ESA}$ due to the presumably large density of states of the conduction band while estimating $\omega_{Em} \approx \omega_{ESA}$. Next we can rewrite $I$ in terms of the resonant photon energy density as

$$I = \frac{\hbar\omega_{Em} c\phi}{V_{mode}} \qquad (4)$$

We can also define an effective cross section $\sigma_{\text{eff}} \cong \sigma_{Em} - \sigma_{ESA}$. Lastly, we can assume that the entire mode volume of the resonator sees gain allowing us to approximate $V_g / V_{mode} \sim 1$. With these simplifications, our model becomes

$$\frac{dN_2}{dt} = R_p - \frac{\sigma_{eff} c}{V_{mode}} \phi N_2 - \Gamma_{21} N_2 \tag{5}$$

$$\frac{d\phi}{dt} = -\frac{\phi}{\tau_c} + \sigma_{eff} c \phi N_2 - \Gamma_{21} N_2 V_{mode} \tag{6}$$

Field Code Changed

Based on Equations 5 and 6, we can determine approximate values for threshold parameters. We first define the threshold to be the point at which the photon number becomes undamped. By inspecting Equation 6, it is apparent that the first two terms decide at which point this occurs. While the third term may implicitly depend on $\phi$ by Equation 5, increasing $\phi$ serves to decrease $N_2$ at first order. Therefore using the first two terms gives a lower bound for the threshold parameters.

To remove the explicit damping of $\phi$,

$$\frac{1}{\tau_c} < \sigma_{eff} c N_2 \tag{7}$$

which implies that

$$N_{2,th} = \frac{1}{\sigma_{eff} c \tau_c} \tag{8}$$

For this to occur, the pumping rate $R_p$ must outweigh the spontaneous emission rate given by $\Gamma_{21} N_2$. Thus

$$R_{p,th} = \frac{\Gamma_{21}}{\sigma_{eff} c \tau_c} \tag{9}$$

For this approximation we used Equation 3 and noted that the stimulated emission is small compared to spontaneous emission prior to reaching the lasing threshold. Carrying on, we find that the threshold intensity and pulse energy are

$$I_{th} = \frac{2\pi hc}{\tau_f Q \sigma_{eff} \sigma_{abs} N_0 \lambda_s \lambda_p} \tag{10}$$

where $\sigma_{abs}$ is the pump laser absorption cross-section; $\lambda_s(\lambda_p)$ is the laser (pump) wavelength; $N_o$ is the $Ce^{3+}$ number density; $\tau_f$ is the lifetime associated with the lasing transition. From literature, we have the laser transition absorption cross-section $\sigma_{Em}$= 9.6 x $10^{-22}$ $m^2$ [9] and the absorption cross-section from the excited 5d level into the host conduction band $\sigma_{ESA}$= 3.6 x $10^{-22}$ $m^2$ [9] . Given typical Q achievable at 1x$10^7$ and higher, and a typical $Ce^{3+}$ concentration of 1 mol%, the theoretically estimated lasing threshold occurs for pump intensity < 1.3 x $10^9$ W/$m^2$, two orders of magnitude lower than that reported in Ref. [11].

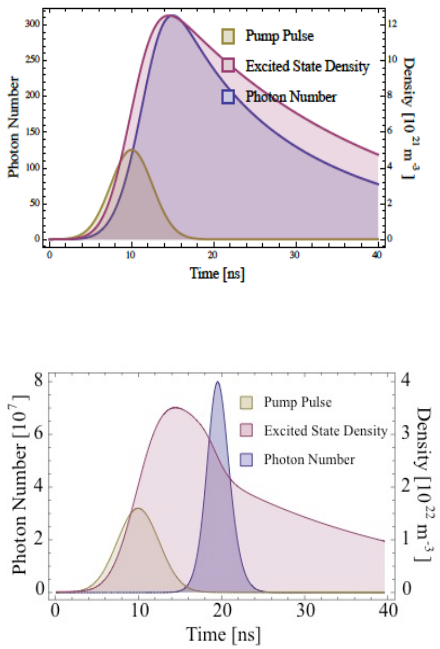


Figure 2: The simulated lasing pulse dynamics above threshold.

We can model the lasing dynamics by studying Equations 5 and 6 in non-steady states. This can be done by solving the equations numerically. Figure 2 shows the resultant photon number (left axis) and the excited state density (right axis) for below and just above threshold condition when the system is pumped with a pulse laser.

Below threshold the photon number is damped because the condition in equation 7 is not satisfied for the majority (if not all) of $t$. This prohibits the onset of strong stimulated emission (due to small photon number) resulting in a tail behavior similar to the excited state density. As the pump energy increases the behavior of $\Phi(t)$ goes from strongly resembling the excited state density behavior to a more peaked function with tail behavior increasingly closer to being described by a $\tau_c$ time constant.

The pump energy first increases the excited state density. The excited state density continues to rise even the short pulse energy starts to decrease till it reaches the threshold such that the stimulated emission outweighs spontaneous emission. This onset is manifested in the increased negative slope in the excited state density in concert with the fast pulse in the photon number. As the excited state density falls, so does the photon number, resulting in the return to the $1/\Gamma_{21}$ tail behavior for the excited state. As will be described below, our initial experimental demonstration used a pulse pump laser. We used the model to simulate laser output and the delay between the pump pulse and the laser pulse as a function of the total pump energy in order to compare with our experimental results.

## 3. EXPERIMENTAL DEMONSTRATION

### 3.1 $Ce^{3+}$:LiCAF WGM resonator fabrication

The WGM resonators used in this work were fabricated from bulk LiCAF and Ce:LiCAF crystalline materials with techniques similar to those described in Ref. [18]. The bulk crystals (AC Materials) were cut into thin disks, preformed, and polished to optical smoothness. The finished resonator disks typically have diameters of 2 – 3 mm and thicknesses of ~100 µm. The UV Q factors of these resonators were initially measured with a 370 nm laser, the only narrow linewidth cw UV laser available in our laboratories. The laser is evanescently coupled to the resonator via a prism and its coupling spectrum is monitored. We determined the resonator Q by measured WGM resonance linewidth. The laser linewidth is about 1 MHz. The measured resonator linewidths are on the order of ???, so they are Q dominated linewidths. Q = 2.6 x $10^7$ and Q = 2 x $10^6$ have been observed for LiCAF and Ce:LiCAF resonators respectively. The lower Q measured for Ce:LiCAF is most likely due to the material absorption at 370 nm though we do not have independent absorption measurements.

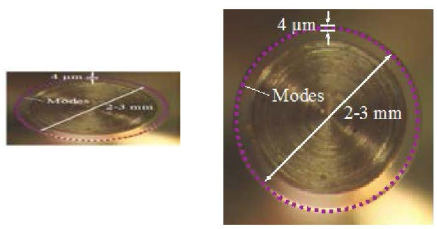


Figure 3: Side and top view images of WGM resonator which were fabricated with $Ce^{3+}$:$LiCaAlF_6$ crystal.

### 3.2 Experiment setup

The WGM resonator laser is most efficiently pumped by a cw laser that is resonantly coupled to WGMs. In this pump configuration, all pump energy is confined in a small WGM mode volume that overlaps well with the laser modes. At present time, we do not have such a cw pump laser around 260 nm. To experimentally verify this lasing threshold, therefore, we used a frequency-quadrupled pulsed Nd:YAG laser (266 nm, 2 mJ at 2 Hz, 6 ns pulse) to pump the Ce:LiCAF WGM resonators. The schematic and experimental setup shown in Fig. 4. Rather than resonantly coupling the pump light through the resonator evanescent field, the pump light is directly focused on the top surface of the resonator disk with a Gaussian spot size maximally overlapped with the WGM. The WGM lasing signal was observed by evanescent wave coupling to a prism and measured with a photodiode and a spectrometer situated behind a set of optical filters to block the 266 nm pump light.

xxx

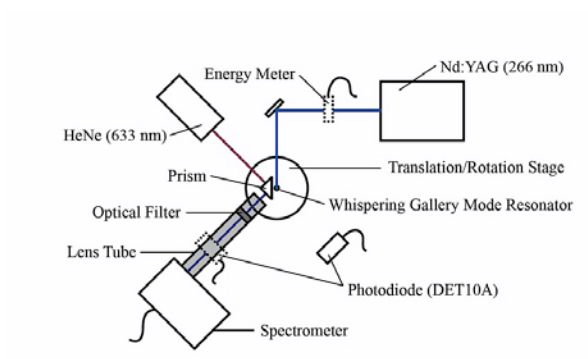

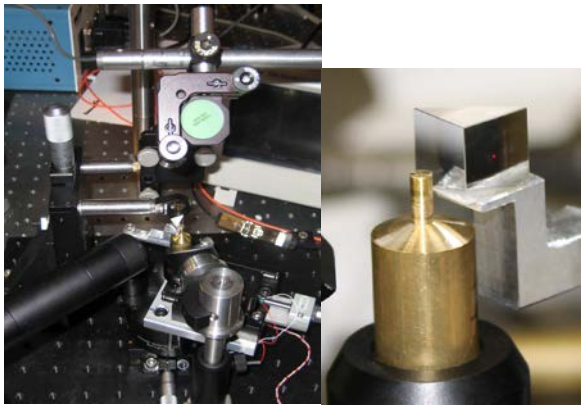

Figure 4: Schematic and setup of the UV laser experiment. The 266 nm pump laser beam is projected from the top of the resonator disk and the lasing signal was evanescent wave coupled to a prism for detection.

### 3.3 Experiment Results

Figure 5 shows the measured out-coupled laser power as a function of pump laser energy. We clearly observed the expected lasing threshold curve, the onset of lasing at about 1.6 µJ. Also shown in Figure 5 is the result of the simple 4-level laser rate equation model described above using a $Ce^{3+}$ number density of $N_o$= 5.5 x $10^{23}$ $m^{-3}$ and probability of spontaneous emission into the laser mode of $\beta$ ~ 0.01. The lasing threshold observed in Figure 5 corresponded to an applied total pump energy of 800 µJ. Due to mismatch between the pump laser spatial mode and the WGM lasing modes as well as small thickness of the disk, only a small fraction of this pump energy was actually absorbed in the gain medium. Calculating this fraction and the actual pump intensity in the WGM volume requires knowledge of the WGM laser profile inside the crystal resonator, where the lasing modes reside. In the present experiment we cannot differentiate the various lasing modes, however, typically only equatorial WGMs contribute to the observed lasing signal as they exhibit the highest Q and are more strongly out-coupled via the prism.

**Formatted:** Font color: Light Blue

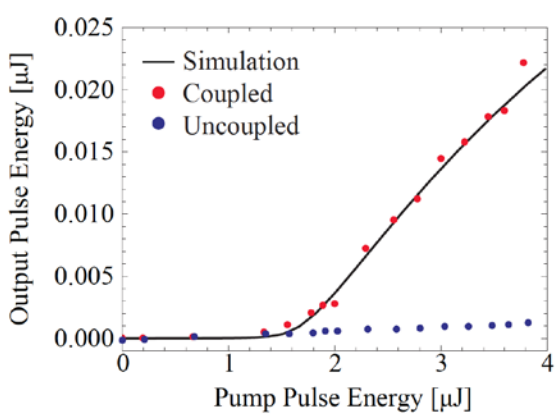


Figure 5: Experimental and simulated laser output as a function of the total pump energy, showing the lasing threshold of 1.6 µJ.

Assuming equatorial WGMs, we find that the fraction of the pump pulse energy that is incident upon the volume containing the lasing modes is 0.002, leading to an actual pump energy threshold of 1.6 μJ as shown in Fig 3. This corresponds to a laser threshold pump intensity of 7.5 x $10^9$ W/$m^2$. The theoretically estimated laser threshold based on the description in the previous section is 1.35 x $10^9$ W/$m^2$. The measured threshold value is consistent with the theoretical estimate when we consider that the definition for the threshold intensity is the intensity at which the resonant photon number becomes undamped, whereas the measured threshold intensity is taken to be the intensity at which the photon number becomes experimentally measureable and increases linearly with pump power.

Taking into account geometric factors and losses, the overall slope efficiency is found to be 1.1% in this top-pumped configuration. However, due to an absorption coefficient of $\alpha$ = 4.1 cm-1 only ~4% of the pump energy incident upon the mode volume is absorbed in the 100 μm thick active medium, resulting in an effective slope efficiency of ~25% when the pump can be mostly absorbed. The ttoal pupo absorption can be most readily realized in a resonant coupled pump geometry. To further validate the output light is the lasing light resonantly coupled out from the resonator, we observe the detected signal when the resonator is uncoupled from the prism by increasing their separation by ~100 μm. This signal is found to be negligible and without threshold behavior as also shown in Figure 5, which implies that the signal in the coupled configuration is due to out-coupled resonant photons as opposed to incoherent fluorescence from the resonator.

Figure 6 shows the spectrum of the UV WGM laser for several pump energies using a UV spectrometer with ~0.1 nm resolution. Consistent with previous observations [10], the laser displayed a dominant emission peak centered at 286 nm with a secondary peak around 310 nm, showing that both tunable cw and mode-locked operation in the WGM laser are possible in principle. Finally, a control experiment was also performed using an undoped LiCAF host in the same setup, which confirmed that no spurious emission from the crystal contaminated the measured laser spectrum.

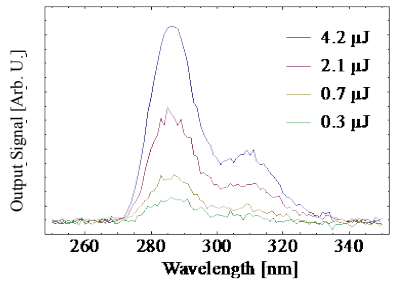


Figure 6: UV WGM laser spectrum at several pump energies.

As discussed in the previous section in pulsed mode operation, the competition between the creation of an inversion by the pump pulse and the depletion of the inversion by the lasing pulse leads to rich dynamics in the time domain, which has been explored in Ref. [13]. The result from the simple four-level rate equation model of the laser time dynamics is shown in Figure 2, where it is shown that there is a finite time for the gain medium to build up the population inversion. The build-up time is pump power dependent, as it is relatd to the total accumulated excited state density. Once sufficient inversion is reached, the number of laser photons rapidly increases, resulting in the sudden overtaking of spontaneous emission by stimulated emission and a marked decrease in excited state density (Fig. 4). Together these effects lead to a time delay between the pump pulse and the laser pulse that depends on the total pump energy. We have measured this delay dependence on pump energy and it is shown in Figure 7 alongside the result of the simple rate equation model. Considering the idealization of the four-level model, the agreement is reasonable. However, the fact that the experimental data shows a peak time delay at larger energies, as well a slower decrease in delay with energy, compared to simulation indicates that the simulation may be overestimating the real excited state density participating in the observed lasing signal.

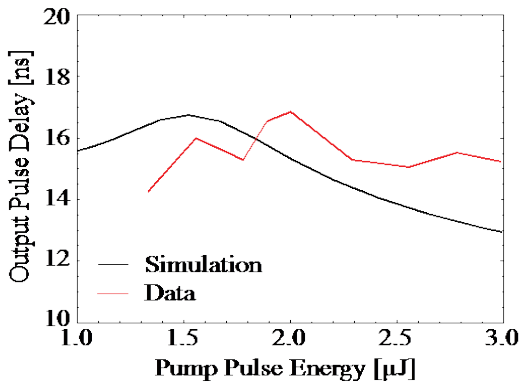


Figure 7: Experimental and simulated delays as a function of the pump energy.

## 4. CONCLUSION

In summary, we have fabricated and experimentally demonstrated a low threshold UV lasers based on solid state WGM $Ce^{3+}$: $LiCaALF_6$ crystalline resonators. With a $Ce^{3+}$:$LiCaAlF_6$ resonator pumped by a 266 nm pulsed laser, we observed the operation of a wide-bandwidth laser (280 nm – 330 nm) with a threshold intensity of 7.5 x $10^9$ W/$m^2$ and an effective slope efficiency of ~25%. Based on a simple 4-level laser modeling with coupled rate equations, we can estimate the laser threshold as well as simulate the lasing dynamics. These results suggests that there is significant potential for further reducing the lasing threshold. For example, if a narrow-band 266 nm pump laser is resonantly coupled to a WGM resonator similar in size to those used in our current experiment, the pump mode almost completely overlaps the laser mode volume. This can be accomplished by reducing the dopant concentration so as to have a reasonable resonator Q of. $10^7$, at the pump wavelength. This may be counter intuitive. The decrease in total pump photon absorption due to the smaller dopant concentration is actually compensated by the corresponding cavity buildup of the pump intensity inside the resonator. The resonantly coupled pump also allows the complete absorption of pump by the gain medium as it is this absorption that dominates the Q value at the pump This pump coupling configuration, with the demonstrated LiCAF resonators Q of $10^7$, results in a predicted cw laser pump power threshold as low as 20 mW. The proof-of-concept demonstration of UV laser which based on WGM $Ce^{3+}$: $LiCaALF_6$ crystalline resonators leads to a possible platform for investigation of low threshold cw UV lasers. Currently, we are pursuing the development of such a device in an effort to enable both tunable cw and mode-locked operation in the UV spectral range.

## ACKNOWLEDGEMENTS

Part of this work was performed at the Jet Propulsion Laboratory, California Institute of Technology, under a contract with NASA. The research is supported in part by JPL Strategic University Research Partnerships Program. UCLA also acknowledges support from the DARPA QuASAR program.

## REFERENCES


[1] M. Maeda, T. Sibata, and H. Akiyoshi, **"**Optimum wavelengths in solar-blind UV ozone lidars,**"** Japanese Journal of Applied Physics 29, 2843–2846 (1990).

[2] Viktor A. Fromzel, Coorg R. Prasad, Karina B. Petrosyan, Yishinn Liaw, Mikhail A. Yakshin, Wenhui Shi, and Russell DeYoung, "Tunable, Narrow Linewidth, High Repetition Frequency Ce:LiCAF Lasers Pumped by the Fourth Harmonic of a Diode-Pumped Nd:YLF Laser for Ozone DIAL Measurements," Advances in Optical and Photonic Devices, Book edited by: Ki Young Kim, (2010).

[3] P J Hargis, T J Sobering, G C Tisone, J S Wagner, S A Young, R J Radloff, "Ultraviolet fluorescence detection and identification of protein, DNA, and bacteria," SPIE 2366, 147-156 (1995).

[4] T. Rosenband, D. B. Hume, P. O. Schmidt, C. W. Chou, A. Brusch, L. Lorini, W. H. Oskay, R. E. Drullinger, T. M. Fortier, J. E. Stalnaker, S. A. Diddams, W. C. Swann, N. R. Newbury, W. M. Itano, D. J. Wineland, J. C. Bergquist, "Frequency Ratio of $Al^+$ and $Hg^+$ Single-Ion Optical Clocks; Metrology at the $17^{th}$ Decimal Place," Science 319, 1808 – 1812 (2008).

[5] W.G. Rellergert, D. DeMille, R.R. Greco, M.P. Hehlen, J.R. Torgerson, E.R. Hudson, "Constraining the Evolution of the Fundamental Constants with a Solid-State Optical Frequency reference Based on the $^{229}$Th Nucleus," Phys. Rev. Lett. 104, 200802 (2010).

[6] E. Peter, S.A. Diddam, P. Fendel, S. Reinhardt, T. W. Hansch, Th. Udem, "A deep-UV optical frequency comb at 205 nm," Optics Express 17(11), (2009).

[7] Nan Wang, Rui Wang, Hao Teng, Dehua Li, Zhiyi Wei, "Tunable deep UV narrow linewidth laser by frequency converted Ti:sapphire Laser at 5kHz repetition rate," Lasers, Sources, and Related Photonic Devices Technical Digest (2012).

[8] D. W. Coutts and A. J. S. McGonigle, "Cerium-doped fluoride lasers," IEEE J. Quantum Electron. 40, 1430-1440 (2004).

[9] C. D. Marshall, J. A. Speth, S. A. Payne, W. F. Krupke, G. J. Quarles, V. Castillo, and B. H. T. Chai, "Ultraviolet laser emission properties of Ce3+-doped $LiSrAlF_6$ and $LiCaAlF_6$," J. Opt. Soc. Am. B 11, 2054-2065 (1994).

[10] H. Liu, D. J. Spence, D. W. Coutts, H. Sato and T. Fukuda, "Low-threshold broadly tunable miniature cerium lasers," in OSA Topical Meeting on Advanced Solid-State Photonics (ASSP), OSA Technical Digest (2006).

[11] D. Alderighi, G. Toci, M. Vannini, D. Parisi, S. Bigotta, and M. Tonelli, "High Efficiency UV Solid State Lasers Based on Ce:$LiCaAlF_6$ Crystals," Appl. Phys. B 83, 51 – 54 (2006).

[12] E. Granados, D. W. Coutts, and D. J. Spence, "Deep ultraviolet diamond Raman laser," Optics Express 19(11), 10857-10863 (2011).

[13] D. Alderighi, G. Toci, M. Vannini, D. Parisi and M. Tonelli, "Experimental evaluation of the cw lasing threshold for a Ce:$LiCaAlF_6$ laser," Optics Express 13(19), 7256-7264 (2005).

[14] V. Sandoghdar, F. Treussart, J. Hare, V. Lefèvre-Seguin, J.-M. Raimond, and S. Haroche, "Very low threshold whispering-gallery-mode microsphere laser," Physical Review A 54(3), R1777- R1780 (1996).

[15] H.-S. Hsu, C. Cai, A. M. Armani, "Ultra-low threshold Er:Yb sol-gel microlaser on silicon," Optics Express 17(25), 23265 - 23271 (2009).

[16] E. Ostby and K. Vahala, "Yb-doped glass microcavity laser operation in water," Optics Letters 34, 1153-1155 (2009).

[17] Siyka I. Shopova, Hongying Zhou, and Xudong Fan, and Po Zhang, "Optofluidic ring resonator based dye laser," Applied Physics Latters 90, 221101, (2007).

[18] A.B. Matsko, A.A. Savchenkov, D. Strekalov, V.S. Ilchenko, N. Yu, and L. Maleki, "Fabrication, Characterization and Applications of Crystalline Whispering Gallery Mode Resonators," $9^{th}$ International Conference on Transparent Optical Networks, 50-54, (2007).

[19] http://www.coherent.com